Influence of an electric field on the non-Newtonian response of a hybrid-aligned nematic cell under shear flow

A. David Guillén and Carlos I. Mendoza[a)]
Instituto de Investigaciones en Materiales, Universidad Nacional Autónoma de México, Apartado Postal 70-360, 04510 México, Distrito Federal, Mexico

(Received 23 January 2007; accepted 25 April 2007; published online 30 May 2007)

The authors study shear flow in hybrid-aligned nematic cells under the action of an applied electric field by solving numerically a hydrodynamic model. The authors apply this model to a flow-aligning nematic liquid crystal (4′-*n*-pentyl-4-cyanobiphenyl) and obtain the director's configuration and the velocity profile at the stationary state. The authors calculate the local and apparent viscosities of the system and found that the competition between the shear flow and the electric field gives rise to an interesting non-Newtonian response with regions of shear thickening and thinning. The results also show an important electrorheological effect ranging from a value a bit larger than the Miesowicz viscosity η_b [Nature (London) **17**, 261 (1935)] for small electric fields and large shear flows to η_c for large electric fields and small shear flows. The analysis of the first normal stress difference shows that for small negative shear rates, the force between the plates of the cell is attractive, while it is repulsive for all other values of shear rates. However, under the application of the electric field, one can modify the extent of the region of attraction. Finally, the authors have calculated the dragging forces on the plates of the cell and found that it is easier to shear in one direction than in the other.
 [DOI: 10.1063/1.2741548]

I. INTRODUCTION

Liquid crystals (LCs) are materials highly interesting from a fundamental point of view due to their intriguing symmetries and unusual elastic properties. At the same time, they have found many technological applications and are now routinely employed in many engineering devices. These materials are a well known example of viscoelastic fluids with unique flow properties.[1–4] Although some of these properties are known for a long time, they continue to attract the attention and interest of the scientists. As a result, a large amount of theoretical, numerical, and experimental work has been produced in recent years. In particular, a number of publications treat the behavior of nematic liquid crystals in shear and Poiseuille flow fields.[5–11] These materials show a marked non-Newtonian behavior that arises due to the coupling between the molecular ordering, described by the director field, and the flow field (the so-called backflow).[12,13]

Like in most materials, many important properties depend on the structure of inhomogeneities and interfaces in the liquid crystal. For example, the alignment of nematic liquid crystals by surfaces plays a key role in the liquid crystal display technology. One of the common geometries used in devices is that of the hybrid-aligned nematic (HAN) cell. In this geometry, the alignment of the director field is homeotropic (perpendicular to the surface) at one of the boundaries of the containing cell and at the other is homogeneous (parallel to the surface). Detailed measurements of backflow effects on a HAN cell have been performed and reported in Refs. 14 and 15. On the theoretical grounds, the rheology of this geometry has recently been numerically investigated in Refs. 12 and 13. Due to the conflicting anchoring of a HAN cell, the system adopts a uniform deformation across the sample in trying to minimize its elastic free energy. It has been shown that the interplay between such a distorted director field and the flow field leads to unexpected non-Newtonian behavior. In particular, it has been shown that the elastic distortion strongly affects the velocity profile and introduces an asymmetry.[12]

On the other hand, the influence of electric fields on the rheology of liquid crystals has taken considerable interest due to its possible application in microsystems.[16] In these applications, liquid crystals are used as a fluid whose apparent viscosity can be controlled by an electric field. These electrorheologic properties are revealed to be interesting for many industrial applications. One of the main advantages of electrorheologic liquid crystals over other active fluids is that they do not contain suspended particles. This homogeneity is of particular importance for microsystems since small channels are easily obstructed by suspended particles.[16] In addition, the homogeneity of liquid crystals prevents agglomeration, sedimentation, and abrasion problems.

Static and dynamic flow characteristics of liquid crystals and their electrorheological properties have been treated in a number of papers.[16–22] Some of these papers investigate flows with a constant shear rate over the height of the channel,[17,19,20] while others treat the case of parabolic velocity profiles[16,18] or oscillatory squeeze flow.[22] However, in all of these papers the studies have focused on situations in which the anchoring was the same at all boundaries and the electrorheology of HAN cells was not treated.

[a)]Author to whom correspondence should be addressed. Tel: +52(55)56224644; Fax: +52(55)56161201. Electronic mail: cmendoza@iim.unam.mx

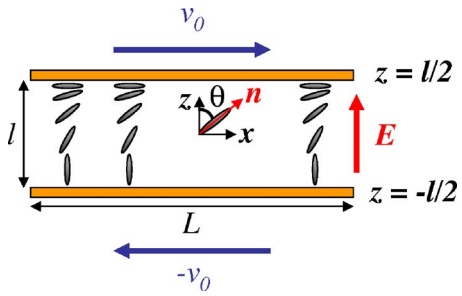

FIG. 1. Schematics of a HAN cell subjected to a normal electric field and a shear stress.

The purpose of the present work is to study theoretically the static characteristics of a HAN cell under the simultaneous action of a shear flow and a perpendicularly applied low-frequency electric field. Our model is based on the Ericksen-Leslie-Parodi approach in contrast to Refs. 12 and 13 where the Beris-Edwards formulation of nematodynamics was employed.[4] Nonetheless, our results can be compared to those of Refs. 12 and 13 in the case of zero electric field. The paper is organized as follows. In Sec. 2, we introduce the model and the governing equations of motion for the liquid crystal cell. In Sec. III, we present the method of solution of the governing equations in order to obtain the stationary solution for the director's field. Then, in Sec. IV, we show the results for the specific case of the flow-aligning liquid crystal 4′-*n*-pentyl-4-cyanobiphenyl (5CB). We calculate the director's orientation, velocity field, viscosity, first normal stress difference, and shear stress. Finally, Sec. V is devoted to conclusions.

II. MODEL AND GOVERNING EQUATIONS

Consider a thermotropic nematic layer of thickness l confined between two parallel plates, as depicted in Fig. 1. The transverse dimensions L of the cell are large compared to l and the cell is under the action of a perpendicular low-frequency electric field. Under these conditions, the director's configuration $\mathbf{n}$ is spatially homogeneous along the x and y directions so that

$$\hat{\mathbf{n}} = [\sin\theta(z), 0, \cos\theta(z)], \tag{1}$$

where $\theta(z)$ is the orientational angle defined with respect to the z axis, as shown in Fig. 1. We shall assume that the orientational angle satisfies strong anchoring conditions at the plates,

$$\theta(z = -l/2) = 0, \quad \theta(z = l/2) = \pi/2. \tag{2}$$

In addition to the electric field, we assume that the plates may move relative to each other to produce a shear flow in the x-z plane and along the x direction (see Fig. 1). Then, the only relevant component of the velocity field is v_x so that

$$\mathbf{v} = [v_x(z), 0, 0], \tag{3}$$

which satisfies the nonslip boundary conditions

$$v_x(z = \pm l/2) = \pm v_0. \tag{4}$$

A common approach to describe the flow of rod shaped LCs is the theory of Ericksen, Leslie, and Parodi.[1] In this formulation, the flow of LCs is described by a stress tensor σ_{ij}, the director $\mathbf{n}$, and the Leslie viscosity coefficients $\alpha_1 - \alpha_6$ as follows:

$$\sigma_{ij} = \alpha_1 n_i n_j V_{kp} n_k n_p + \alpha_2 n_j N_i + \alpha_3 n_i N_j + \alpha_4 V_{ij} + \alpha_5 n_j V_{ik} n_k + \alpha_6 n_i V_{jk} n_k, \tag{5}$$

with

$$V_{ij} = \frac{1}{2}\left(\frac{\partial v_i}{\partial x_j} + \frac{\partial v_j}{\partial x_i}\right), \tag{6}$$

the symmetric part of the velocity gradient tensor, and

$$N_i = \frac{dn_i}{dt} - \frac{1}{2}\left(\frac{\partial v_i}{\partial x_j} - \frac{\partial v_j}{\partial x_i}\right) n_j, \tag{7}$$

the rotation of the director relative to the fluid. In these equations, x_i is a Cartesian coordinate and only five of the six Leslie coefficients are independent due to the Parodi equation

$$\alpha_2 + \alpha_3 = \alpha_6 - \alpha_5. \tag{8}$$

From the above theory, we obtain the torque acting on a sheared molecule,

$$\mathbf{T}_v = \hat{\mathbf{n}} \times \left[\left(\frac{\alpha_3 - \alpha_2}{2} \nabla \times \mathbf{v}\right) \times \hat{\mathbf{n}} - (\alpha_6 - \alpha_5)\mathbf{V} \cdot \hat{\mathbf{n}}\right]. \tag{9}$$

In the two-dimensional situation of interest, the shear torque acting on a molecule can be simplified to[16]

$$T_v = (\alpha_3 \sin^2\theta - \alpha_2 \cos^2\theta)\frac{dv_x}{dz}. \tag{10}$$

Although several publications assume the contribution of α_3 to be negligible, it has been shown[16] that it should be taken into consideration in some situations as, for example, in planar-aligned cells. Therefore, in this study α_3 will not be neglected.

A second torque that acts on the LC molecules is due to the electric field. This field induces an electric dipole in the molecules which makes them turn. In this case, the torque caused by the electric field can be described by

$$T_{el} = -\frac{\varepsilon_a \varepsilon_0}{2} E^2 \sin(2\theta), \tag{11}$$

with ε_0 the permittivity of the vacuum and $\varepsilon_a = \varepsilon_\parallel - \varepsilon_\perp$ the dielectric anisotropy of the LC, $\epsilon_\parallel$ and $\epsilon_\perp$ being the parallel and perpendicular dielectric constants of the LC, respectively.

Elastic deformations in the LC also create torques on the molecules of the LC. The elastic energy is given by the Frank-Oseen expression

$$F_e = \tfrac{1}{2}[K_1(\nabla \cdot \hat{\mathbf{n}})^2 + K_2(\hat{\mathbf{n}} \cdot \nabla \times \hat{\mathbf{n}})^2 + K_3(\hat{\mathbf{n}} \times \nabla \times \hat{\mathbf{n}})^2], \tag{12}$$

where K_1, K_2, and K_3 refer to the splay, twist, and bend deformations, respectively. From this equation the elastic torque can be derived, giving as a result

$$T_e = (K_1 \sin^2\theta + K_3 \cos^2\theta)\left(\frac{d^2\theta}{dz^2}\right) + (K_1 - K_3)\sin\theta\cos\theta\left(\frac{d\theta}{dz}\right)^2. \quad (13)$$

Finally, in the case of dynamic situations, a torque due to rotational inertia and a torque due to viscous damping must be taken into account, leading to the following result:

$$T_{\mathrm{dyn}} = I\frac{d^2\theta}{dt^2} + \gamma\frac{d\theta}{dt}, \quad (14)$$

with I the rotational inertia, γ the viscous damping, and t the time.

All the above contributions result in the differential equation that describes the equilibrium of torques:

$$I\frac{d^2\theta}{dt^2} + \gamma\frac{d\theta}{dt} = (K_1 \sin^2\theta + K_3 \cos^2\theta)\left(\frac{d^2\theta}{dz^2}\right) + (K_1 - K_3)\sin\theta\cos\theta\left(\frac{d\theta}{dz}\right)^2 - \frac{\varepsilon_a\varepsilon_0}{2}E^2\sin(2\theta) + (\alpha_3 \sin^2\theta - \alpha_2\cos^2\theta)\frac{dv_x}{dz}. \quad (15)$$

A last torque acting on the molecules is due to the interaction with the plates of the cell. This contribution is taken into account by the boundary conditions that we are assuming as fixed.

This equation is completed by the linear momentum conservation equation given by[23]

$$\frac{d}{dz}\left[\eta(\theta)\frac{dv_x}{dz}\right] = 0, \quad (16)$$

where

$$\eta(\theta) = \alpha_1 \sin^2\theta\cos^2\theta + \eta_b \sin^2\theta + \eta_c\cos^2\theta \quad (17)$$

is the position dependent viscosity of the LC. In this equation, $\eta_b=(\alpha_3+\alpha_4+\alpha_6)/2$ and $\eta_c=(\alpha_4+\alpha_5-\alpha_2)/2$ are two of the three Miesowicz viscosities.[24] It is interesting to compare our model with that of Refs. 17 and 18. In contrast to the cited works, our model does not neglect α_3 in Eq. (15). Also, in Ref. 17 a constant shear rate over the height of the cell was assumed, instead of the velocity field given by Eq. (16).

III. METHOD OF SOLUTION

The above presented model describes the dynamic behavior of the HAN cell by means of Eqs. (15) and (16). However, in this work we are only interested in the final stationary state of the system. Therefore, the problem now consists in solving this set of simultaneous differential equations in the steady-state regime. To this purpose we first define the normalized variables $\varsigma \equiv z/l$ and $\tilde{v}_x \equiv v_x/|v_0|$ so that Eq. (15) reduces to

$$\frac{d^2\theta}{d\varsigma^2} - \frac{\varepsilon_a\varepsilon_0}{2K}l^2E^2\sin(2\theta) + \frac{l|v_0|}{K}(\alpha_3\sin^2\theta - \alpha_2\cos^2\theta)\frac{d\tilde{v}_x}{d\varsigma} = 0, \quad (18)$$

where we have assumed the equal elastic constant approximation $K_1=K_3=K$. Similarly, after integration Eq. (16) reduces to

$$\frac{d\tilde{v}_x}{d\varsigma} = \mathrm{sgn}(v_0)\frac{c}{\eta(\theta)}, \quad (19)$$

with $\mathrm{sgn}(x)$ the signum function and $c(q,m)$ a positive integration constant that depends only on the electric field and the shear rate and is given by

$$c(q,m) = \frac{2}{\int_{-1/2}^{1/2} d\varsigma'/\eta[\theta(\varsigma')]}. \quad (20)$$

The boundary conditions in terms of the normalized variables take the form

$$\theta(\varsigma = -1/2) = 0, \quad \theta(\varsigma = 1/2) = \pi/2, \quad (21)$$

and

$$\tilde{v}_x(\varsigma = \pm 1/2) = \pm\,\mathrm{sgn}(v_0). \quad (22)$$

Then, we substitute Eq. (19) into Eq. (18) to obtain

$$\frac{d^2\theta}{d\varsigma^2} - q\sin(2\theta) + \frac{m}{\eta(\theta)}(\alpha_3\sin^2\theta - \alpha_2\cos^2\theta) = 0, \quad (23)$$

where we have defined a dimensionless field strength

$$q \equiv \frac{\varepsilon_a\varepsilon_0}{2K}l^2E^2 \quad (24)$$

and the dimensionless shear rate

$$m \equiv \frac{lv_0c(q,m)}{K}. \quad (25)$$

Notice that q takes only positive values, while m is positive if the upper plate of the cell moves to the right (see Fig. 1) and negative if it moves to the left. Also, note that m and v_0 are not linearly related due to the factor $c(q,m)$. Finally, Eq. (23) can be solved numerically using the "shooting" method[25] to obtain the stationary configuration of the nematic's director.

IV. RESULTS

In what follows, the numerical calculations are performed for 5CB. The Leslie coefficients for this LC at $T=25\ ^\circ\mathrm{C}$ are $\alpha_1=-0.0060$ Pa s, $\alpha_2=-0.0812$ Pa s, $\alpha_3=-0.0036$ Pa s, $\alpha_4=0.0652$ Pa s, $\alpha_5=0.0640$ Pa s, and $\alpha_6=-0.0208$ Pa s, and the elastic constant was taken to be $K=12$ pN.

A. Nematic's director configuration

Let us first consider the orientational profile. In Fig. 2 we plot the orientational angle θ vs ς_1 as obtained from Eq. (23) for various values of the parameters q and m. We observe that θ decreases as we increase the value of q. This is in agreement with the tendency of the molecules to be aligned

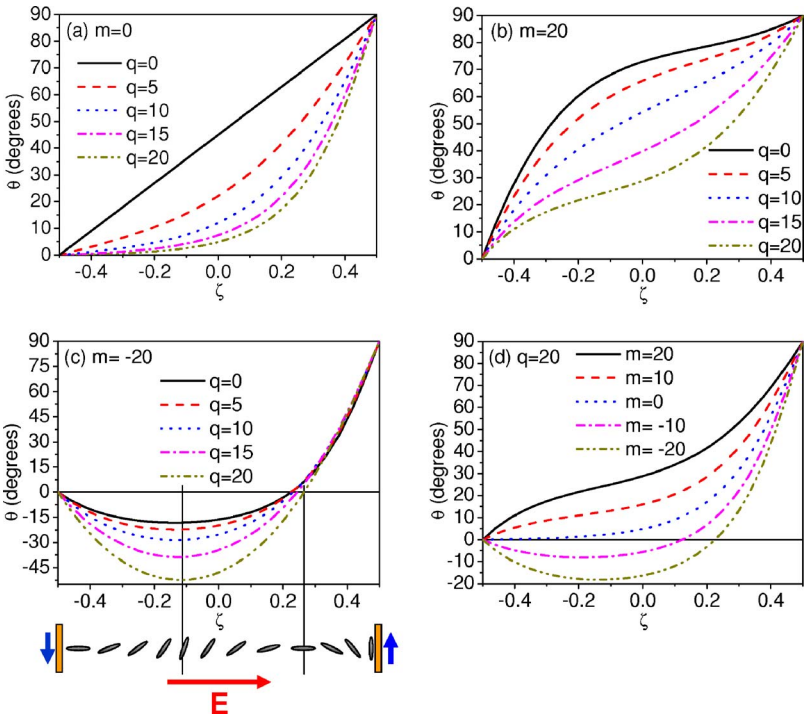

FIG. 2. Nematic's configuration θ as a function of ς for 5CB at $T=25\ ^{\circ}\mathrm{C}$.

with the direction of the electric field. In contrast, θ increases as the value of m increases for $m>0$. This means that the molecules tend to be aligned with the direction of the flow. However, even for very large flows this alignment is not perfect due to the presence of the term with α_3 in Eq. (23). In fact, for very large flows, Eq. (23) leads to the maximum possible value of the orientational angle,

$$\theta_{\max} = \arctan \sqrt{\frac{\alpha_2}{\alpha_3}}, \tag{26}$$

which gives, for the parameters considered, $\theta_{\max} \simeq 78.1°$.

On the other hand, for negative values of m the difference is remarkable. In this case the cell is divided into two regions. In the first one, located at the lower part of the cell, the molecules are tilted toward the left, while in the second region, located at the upper part of the cell, the molecules are tilted to the right. This behavior is a consequence of two conflicting effects. First, the original nematic's configuration changes from homeotropic alignment at the lower plate to a planar configuration at the upper plate in a clockwise way. Second, for negative values of m, the flow tends to align the molecules trying to rotate them in a counterclockwise way. The effect of the flow dominates near the lower plate, while the effect of the anchoring dominates near the upper plate, giving as a result the two regions. The width of these two regions is almost unaffected by the application of the electric field but depends strongly on the magnitude of the flow.

B. Velocity profile

Integrating Eq. (19) and taking into consideration the nonslip boundary conditions given by Eq. (22), we obtain the following expression for the velocity of the nematic:

$$\tilde{v}_x(\varsigma) = -\operatorname{sgn}(v_0)\left\{1 - 2\frac{\int_{-1/2}^{\varsigma} d\varsigma'/\eta[\theta(\varsigma')]}{\int_{-1/2}^{1/2} d\varsigma'/\eta[\theta(\varsigma')]}\right\}. \tag{27}$$

Once $\theta(\varsigma)$ has been determined numerically from Eq. (23) it can be inserted into Eq. (27) to obtain $\tilde{v}_x(\varsigma)$. The velocity profile for positive shear, $m>0$, is shown in Fig. 3. The velocity is parametrized by the the shear rate m for (a) $q=0$ and (b) $q=20$. We observe that the velocity profile $\tilde{v}_x(\varsigma)$ is very insensitive to the shear rate. However, the shape of the curves is different in the case $q=0$ as compared to the case $q=20$. In the first case the curvature of the profile is larger near the lower plate, while in the second case the profile is almost linear in this region and the curvature increases near the upper plate. To see the effect of the electric field more clearly, in Fig. 4 we show the velocity profile for

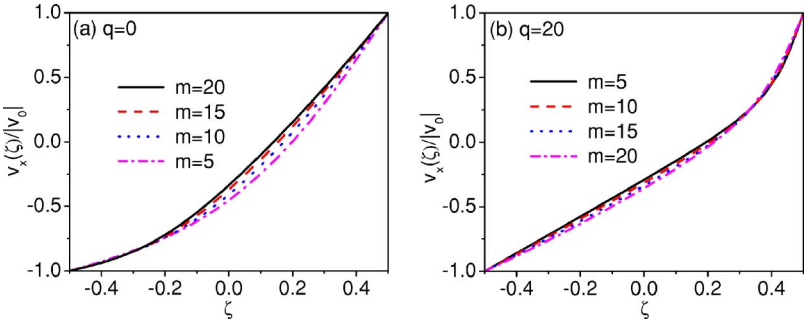

FIG. 3. Velocity profiles $\tilde{v}_x$ vs ς for positive shear rate: (a) $q=0$ and (b) $q=20$.

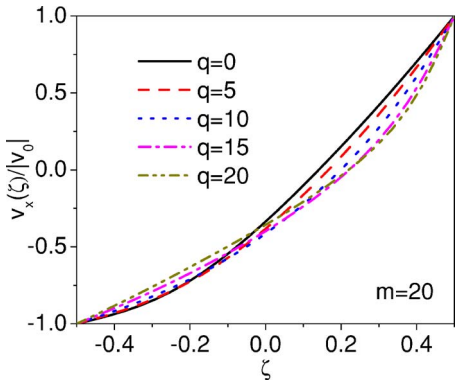

FIG. 4. Velocity profiles $\tilde{v}_x$ vs ς for different values of q, with $m=20$.

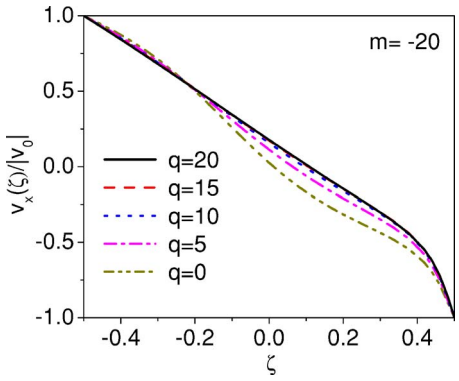

FIG. 6. Velocity profiles $\tilde{v}_x$ vs ς for different values of q, with $m=-20$.

different values of q. Note how the position of the largest curvature moves gradually from a position near the lower plate to a position near the upper plate as we increase the electric field. This is in agreement with the fact that a larger electric field aligns more effectively the molecules of the LC except in the region near the upper plane where we have the largest variation of the director's orientation in order to satisfy the boundary condition at the upper plate. In Fig. 5 we show the velocity profile for negative shears, $m<0$. Note that in this case, the profile is much more sensitive to the shear rate, especially for the case $q=0$. This plot confirms the presence of the two regions since regions of high and low velocity gradients correspond to flow-aligning and homeotropic director's orientation, respectively. This characteristic is more pronounced for larger shear rates. The presence of the electric field renders the transition between the two regions less abrupt, as can be seen in Fig. 6. Also, the asymmetric behavior between the positive and negative shear rate cases is decreased as the electric field is increased. In the case of no applied electric field our results for the velocity profile and the orientational angle are qualitatively similar to those of Refs. 12 and 13 where results for a HAN cell are obtained in the absence of electric field.

In Fig. 7 we have plotted the average velocity given by

$$\langle v_x(q,m)\rangle = \int_{-1/2}^{1/2} v_x(\varsigma;q,m)d\varsigma \tag{28}$$

as a function of m. Note that, in contrast to Newtonian fluids, in all cases the average velocity of the nematic is nonzero, that is, the center of mass of the nematic moves with constant velocity. This is due to the fact that most of the fluid moves following the movement of the lower plate.

C. Viscosity

The position dependent viscosity can be calculated from Eq. (17) and it is shown in Fig. 8. This figure confirms the completely different behavior for positive and negative shear rates. While in the case of positive shear the viscosity decreases monotonically in going from the lower plate to the upper one, for negative shear rates the curves for the viscosity show a nonmonotonic trend with maxima and minima. It is possible to understand qualitatively the general trends of these curves by considering the orientational angle of the nematic's director θ. For positive shears, θ increases from $\theta=0$ at the lower plate to $\theta=\pi/2$ at the upper plate for any value of q. The position dependent viscosity is therefore maximum at the lower plate where the molecules are perpendicularly aligned with respect to the direction of flow and minimum at the upper plate where the molecules are aligned in the direction of flow. Similarly, for negative shear rates, the viscosity is larger for positions in which the molecules are perpendicularly oriented with respect to the direction of the flow and is smaller at the points where the molecules tend to orient with the direction of field. Actually, the value of the viscosity at the points where the molecules are perpendicular to the direction of flow coincides with the value of the Miesowicz viscosity η_c, while the viscosity at the upper plate, where the molecules are parallel to the direction of flow, takes the value η_b. At intermediate points the viscosity takes intermediate values. The intermediate minimum is deeper for larger values of the shear because in this case the molecules are more aligned with the direction of the flow. Under the action of the field, the intermediate minimum becomes shallower because the molecules tend to align with

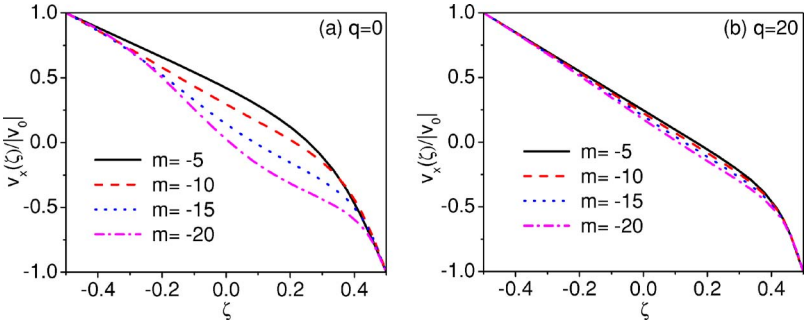

FIG. 5. Velocity profiles $\tilde{v}_x$ vs ς for negative shear rate: (a) $q=0$ and (b) $q=20$.

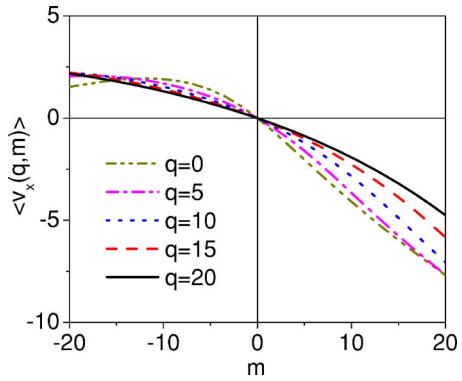

FIG. 7. Average velocity as a function of m.

the direction of the field. From an experimental point of view, it is convenient to measure an average apparent viscosity defined as

$$\langle \eta(q,m) \rangle \equiv \int_{-1/2}^{1/2} \eta[\theta(\varsigma);q,m]d\varsigma. \tag{29}$$

In Fig. 9, we show the apparent viscosity as a function of (a) q and (b) m. The increase of the apparent viscosity as we increase the value of the electric field is evident in panel (a). This electrorheological effect is of moderate intensity since the minimum value that the apparent viscosity may take is $\eta(\theta_{\max})$, when the molecules are oriented with an angle $\theta_{\max}$, that is, almost completely oriented in the direction of the flow, which occurs at large shear rates and small electric fields, and the maximum value that it can take is η_c, when the molecules are perpendicularly aligned with respect to the direction of flow, which occurs for small shear rates and large electric fields. In the present case the minimum and maximum values are $\eta(\theta_{\max}) \simeq 0.024$ Pa s and $\eta_c = 0.1052$ Pa s, respectively. In Fig. 9(b) we plot the viscosity as a function of the shear rate. We observe an interesting non-Newtonian behavior with alternate regions of shear thickening and thinning. The former occurs only for low negative shear rates. This region of shear thickening is the result of the competition between the direction of flow that tends to orientate the molecules in a counterclockwise way and the original director's configuration in which the orientation takes place clockwise. The net result is that the molecules tend to be more vertically aligned than in the case of zero shear. For larger magnitudes of the shear rate, the effect of the flow dominates, producing the shear thinning regions.

D. First normal stress difference

We shall now examine the effects produced by the stresses generated after the reorientation process has taken place by calculating the viscometric functions which relate the shear and normal stress differences. Using the convention of Ref. 26, the first normal stress difference is defined by

$$N_1 \equiv \sigma_{xx} - \sigma_{zz}, \tag{30}$$

where σ_{ii} are the components of the stress tensor given in Eq. (5). This leads to

$$N_1[\theta(\varsigma)] = -\frac{|v_0|}{2l} \sin 2\theta(\alpha_1 \cos 2\theta + \alpha_2 + \alpha_3)\frac{d\tilde{v}_x}{d\varsigma}. \tag{31}$$

In Fig. 10 we plot N_1 vs ς for (a) $q=0$ and (b) $q=20$. As we can see, N_1 is always zero at the plates of the cell and takes only positive values for positive shear rates. In contrast, for negative shear rates, N_1 is positive in the lower part of the cell and negative in the upper part. This asymmetrical behavior with respect to the direction of shear is again a consequence of the asymmetry in the original director's orientation. Notice that the position in which $N_1=0$ corresponds to the point in which the molecules of the nematic adopt a perpendicular or parallel position with respect to the direction of flow. Also, the curves flatten for lower values of the shear rate. Under the action of the electric field the position of the extrema of the curves shifts toward the upper part of the cell in the case of positive shear rate but it is almost unaffected in the case of negative shear rates, as shown in Fig. 11. Also, the size of the region of negative N_1 is slightly

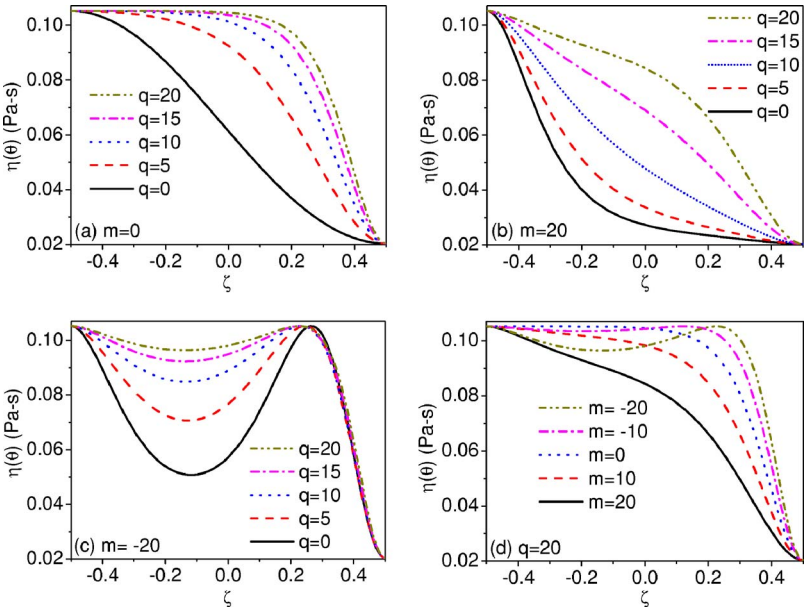

FIG. 8. Local viscosity $\eta(\theta)$ vs ς for different values of q and m.

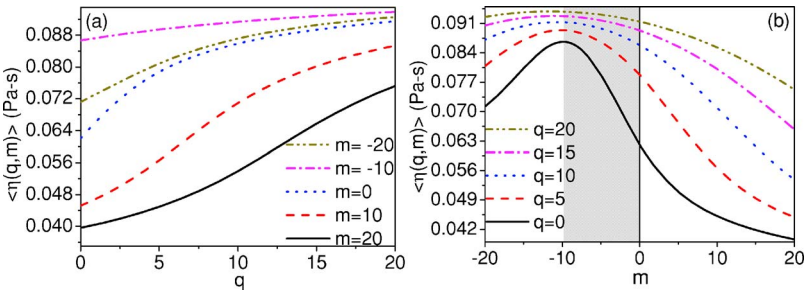

FIG. 9. Averaged apparent viscosity as a function of (a) q and (b) m.

modified by the action of the field. As it is expected, N_1 is identically zero for zero shear, $m=0$.

The integration of the first normal stress difference profile over the cross section of the cell,

$$\langle N_1(q,m)\rangle = \int_{-1/2}^{1/2} N_1[\theta(\varsigma);q,m]d\varsigma, \tag{32}$$

renders the averaged first normal stress difference. Under conditions of shear flow, non-Newtonian fluids show negative steady-state first normal stress difference, $\langle N_1\rangle$, over a range of shear rates. In general, $\langle N_1\rangle$ is zero or positive for isotropic fluids at stationary flows over all shear rates. A positive $\langle N_1\rangle$ means that there is a force due to the normal stresses which tends to separate the two confining surfaces that produce the shear. In liquid crystalline solutions, positive normal stress differences are found at low and high shear rates, while negative values occur at intermediate shear rates.[27] In the latter case, the force tends to joint the confining surfaces. This is shown in Fig. 12, where we have plotted $\langle N_1\rangle$ as a function of (a) q and (b) m. The figure illustrates the quite contrasting difference in the behavior between backward and forward flows. As can be seen, for forward flow $\langle N_1\rangle$ is positive and for backward flow it is negative at low shear rates but is positive at high shear rates. Furthermore, the effect of the electric field is not simple; for example, for positive shear rates, the effect of the field is first to increase the value of $\langle N_1\rangle$, that is, the field increases the repulsive force between the plates of the cell, but then, as we increase the field even more, $\langle N_1\rangle$ starts to decrease again. For negative shear rates the effect is also mixed. In fact, in this latter case, there is a first region at low negative shear rates in which the effect of the field is to decrease the magnitude of $\langle N_1\rangle$, that is, the field decreases the attraction between the plates of the cell. However, there is a second region in which the field makes the value of $\langle N_1\rangle$ more negative, that is, the attraction between the plates of the cell increases or, if $\langle N_1\rangle$ was positive, the repulsion between the cells may become attraction for large enough electric fields. The transition between these two regions occurs in a point that is almost independent of the value of the electric field. In the figure, this value corresponds to $m \simeq -10$.

E. Shear stress

It is also useful to calculate the only nonvanishing stress component σ_{xz} from Eq. (5). We find, after doing similar manipulations to those used to obtain Eq. (31), that

$$\sigma_{xz} = \frac{1}{2}\frac{dv_x}{dz}[2\alpha_1 \sin^2\theta\cos^2\theta + (\alpha_5-\alpha_2)\cos^2\theta + (\alpha_3+\alpha_6)\sin^2\theta + \alpha_4] \tag{33a}$$

$$= \eta(\theta)\frac{dv_x}{dz} \tag{33b}$$

$$= \frac{K}{l^2}m, \tag{33c}$$

where we have used Eqs. (17), (16), and (25). The dragging force per unit area, D_{low} (D_{up}), exerted by the flowing nematic on the lower (upper) plate, is obtained by evaluating σ_{xz} ($-\sigma_{xz}$) on the plate. Since σ_{xz} is independent of z, as seen from Eq. (33c), then the dragging forces on the plates are equal but with opposite signs,

$$D = D_{\text{low}} = -D_{\text{up}} = \frac{K}{l^2}m. \tag{34}$$

This means that the total force that the plates exert on the nematic is zero, which is consistent with the fact that the center of mass of the fluid moves with constant velocity as shown in Sec. IV B. We observe that D has a linear increase as a function of m, but for a fixed m it is independent of q. However, let us point out that this does not mean that the dragging force is independent of the electric field since m also depends on it by means of the relationship given in Eq.

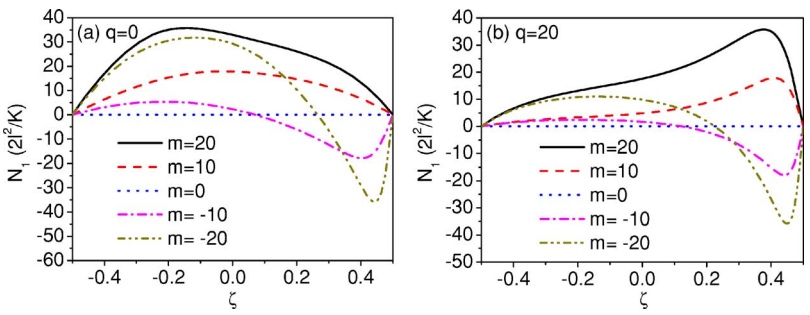

FIG. 10. First normal stress difference N_1 vs ς: (a) $q=0$ and (b) $q=20$.

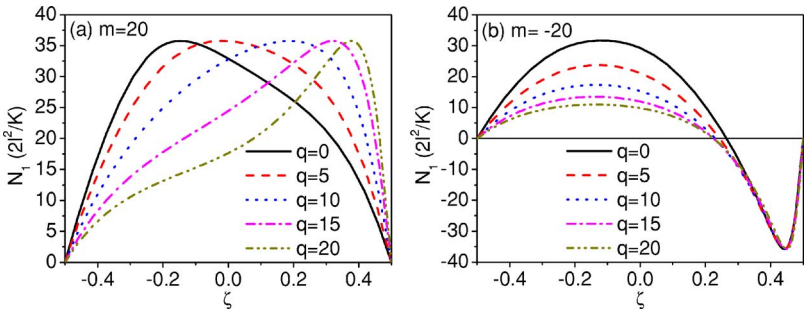

FIG. 11. First normal stress difference N_1 vs ς: (a) $m=20$ and (b) $m=-20$.

(25). In fact, substituting this equation in Eq. (34), we can write

$$D = \frac{K}{l^2}\tilde{\tilde{v}}_0 c(q,m). \tag{35}$$

In Fig. 13 we have plotted the normalized dragging force $\tilde{D}=\tilde{\tilde{v}}_0 c(q,m)$ as a function of the normalized shear velocity $\tilde{\tilde{v}}_0=v_0 l/K$. We can see that the dragging force increases with the magnitude of v_0 and with the value of q. Notice that the magnitude of this force is not the same for v_0 than for $-v_0$, which means that it is easier to shear in one direction than in the other.

V. CONCLUSIONS

We have constructed a hydrodynamic model for a HAN cell subjected to the simultaneous action of a perpendicular electric field and a shear stress. Using the Ericksen-Leslie-Parodi nematodynamics, we have written and solved numerically the exact stationary equations for the director's configuration and velocity profile. The non-Newtonian effects are clearly manifested in the behavior of the velocity profiles that show a remarkable difference with respect to the corresponding Newtonian case. These profiles are asymmetric with respect to the direction of shear. Interestingly, the average velocity of the nematic is nonzero, that is, the center of mass of the nematic moves with constant velocity following the movement of the lower plate. Under the action of the electric field the non-Newtonian behavior is less pronounced.

We have shown that the reorientation produced by the electric field gives rise to an augment in the apparent average viscosity of the LC as a function of the applied electric field (electrorheological effect). This viscosity can be as low as $\eta(\theta_{\max})$ and not larger than η_c. The viscosity is also dependent on the value of the shear rate, giving rise to an interesting non-Newtonian behavior. Even more, the viscosity depends not only on the magnitude of the shear rate but also on the direction of the flow with regions of flow thinning and flow thickening.

Also, we have found that the spatial distribution of the first normal stress difference displays a very different behavior in the case of negative shear rates as compared to the case of positive shear rates. In the first case, regions of positive and negative N_1 are shown in contrast to the case of positive shear rate, in which N_1 is positive at every point in the cell. The extent of these regions is modified by the application of the electric field. From this quantity, we have derived the averaged first normal stress difference and found that it is positive for positive values of the shear rate $(m>0)$ and takes positive and negative values for negative shear rates $(m<0)$. This means that positive shear rates produce repulsion between the plates of the cell, while for negative shear rates the interaction between the plates can be attractive or repulsive. Under the action of the electric field, a repulsive interaction may become attractive.

Finally, we have calculated the dragging forces on the lower and upper plates of the cell and found that they increase with the magnitude of the shear v_0 and with the value of the electric field q. Also, we have found that it is easier to shear in one direction than in the other.

It is important to point out that these directional and non-Newtonian behaviors of the confined liquid crystal are a consequence of the coupling between the velocity field and the undistorted configuration. For this reason, the nematic is able to store more elastic energy in one direction than in the other.

The results presented in this paper apply to flow-aligning nematics. In the case of flow tumbling materials a more complicated behavior is expected since in the steady state the director tilts out of the shear plane and has a significant component along the vorticity direction as shown in Ref. 13 for the case of zero electric field.

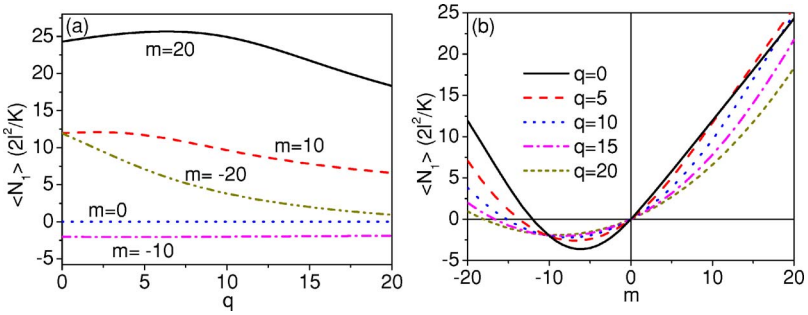

FIG. 12. Averaged first normal stress difference as a function of (a) q and (b) m.

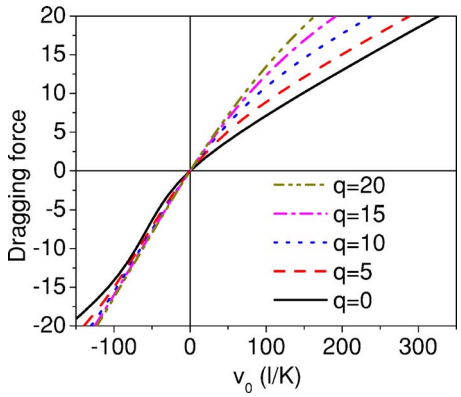

FIG. 13. Dragging force as a function of v_0 for different values of q.

We plan to extend our results to study the dynamics of the system and to treat other geometries such as nematic capillaries under Couette flow or to cells under oscillatory flow. We expect that our results on the non-Newtonian response of the HAN cell and their electrorheological manifestations could stimulate further theoretical and experimental studies, in particular, in microsystems for which these materials are ideally suited.

ACKNOWLEDGMENTS

The authors acknowledge the partial support of DGAPA-PAPIIT Grant Nos. IN-110103 and IN-107607 and CONACYT Grant No. 43596-F.

[1] D. Demus, J. Goodby, G. W. Gray, H.-W. Spiess, and V. Vill, *Handbook of Liquid Crystals* (Wiley-VCH, Weinheim, 1998), Vol. 1.
[2] P. G. de Gennes, *The Physics of Liquid Crystals* (Clarendon, Oxford, 1964).
[3] S. Chandrasekhar, *Liquid Crystals* (Cambridge University Press, Cambridge, 1980).
[4] A. N. Beris and B. J. Edwards, *Thermodynamics of Flowing Systems* (Oxford University Press, Oxford, 1994).
[5] A. D. Rey and M. D. Denn, Annu. Rev. Fluid Mech. **34**, 233 (2002).
[6] W. H. Han and A. D. Rey, Phys. Rev. E **49**, 597 (1994).
[7] P. Toth, A. P. Krekhov, L. Kramer, and J. Peinke, Europhys. Lett. **51**, 48 (2000).
[8] P. Pieranski and E. Guyon, Commun. Phys. (London) **1**, 45 (1976).
[9] E. V. Alonso, A. A. Wheeler, and T. J. Sluckin, Proc. R. Soc. London, Ser. A **459**, 195 (2003).
[10] M. Luskin and T. W. Pan, J. Non-Newtonian Fluid Mech. **42**, 369 (1992).
[11] I. Zuniga and F. M. Leslie, Europhys. Lett. **9**, 689 (1989).
[12] D. Marenduzzo, E. Orlandini, and J. M. Yeomans, Europhys. Lett. **64**, 406 (2003).
[13] D. Marenduzzo, E. Orlandini, and J. M. Yeomans, J. Chem. Phys. **121**, 582 (2004).
[14] S. A. Jewell and J. R. Sambles, J. Appl. Phys. **92**, 19 (2002).
[15] S. A. Jewell and J. R. Sambles, Appl. Phys. Lett. **82**, 3156 (2003).
[16] M. De Volder, K. Yoshida, S. Yokota, and D. Reynaerts, J. Micromech. Microeng. **16**, 612 (2006).
[17] J. A. Reyes, O. Manero, and R. F. Rodriguez, Rheol. Acta **40**, 426 (2001).
[18] R. F. Rodriguez, J. A. Reyes, and O. Manero, J. Chem. Phys. **110**, 8197 (1999).
[19] K. Negita, J. Chem. Phys. **105**, 7837 (1996).
[20] K. Negita, C. Kawano, and K. Moriya, Phys. Rev. E **70**, 021702 (2004).
[21] J. T. Gleeson and W. van Saarloos, Phys. Rev. A **44**, 2588 (1991).
[22] T. Narumi, H. See, Y. Yamaguchi, and T. Hasegawa, JSME Int. J., Ser. B **48**, 524 (2005).
[23] M. Kleman and O. Lavrentovich, *Soft Matter Physics* (Springer-Verlag, New York, 2003).
[24] M. Miesowicz, Nature (London) **17**, 261 (1935).
[25] W. H. Press, B. P. Flannery, S. A. Teukolsky, and W. T. Vetterling, *Numerical Recipes in FORTRAN: The Art of Scientific Computing* (Cambrige University Press, Cambridge, 1986).
[26] R. B. Bird, R. C. Armstrong, and O. Hassager, *Dynamics of Polymeric Liquids* (Wiley, New York, 1977), Vol. 1.
[27] G. Kiss and R. S. Porter, J. Polym. Sci., Polym. Symp. **65**, 193 (1978).